CONF-9207192--1

LA-UR- 92-1442

Title: LOW ENERGY NEUTRAL ATOMS IN THE EARTH'S MAGNETOSPHERE: MODELING

LA-UR--92-1442

DE92 013240

Author(s): K.R. Moore, D.J. McComas, H.O. Funsten, and M.F. Thomsen

Submitted to: SPIE's 1992 International Symposium on Optical Applied Science and Engineering, San Diego, CA 19-24 July 1992

MASTER

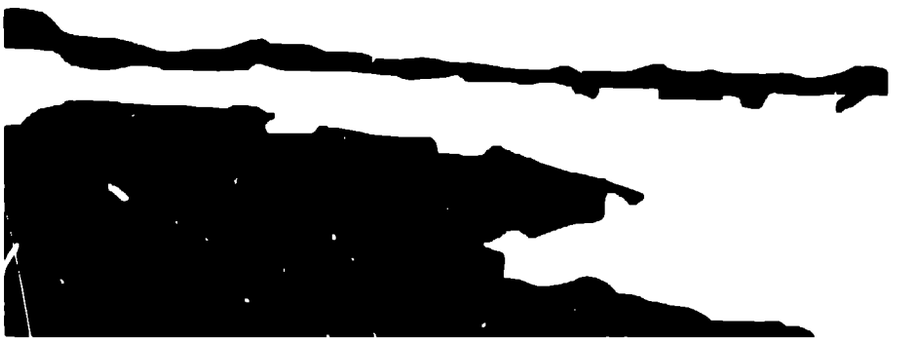

Los Alamos
NATIONAL LABORATORY

Low energy neutral atoms in the Earth's magnetosphere: modeling

Kurt R. Moore
David J. McComas
Herbert O. Funsten
Michelle F. Thomsen

Los Alamos National Laboratory
SST-8 / D438
Los Alamos, NM 87545

ABSTRACT

Detection of low energy neutral atoms (LENAs) produced by the interaction of the Earth's geocorona with ambient space plasma has been proposed as a technique to obtain global information about the magnetosphere. Recent instrumentation advances reported previously[1] and in these proceedings (McComas et al., Funsten et al.) provide an opportunity for detecting LENAs in the energy range of <1 keV to ~50 keV. In this paper, we present results from a numerical model which calculates line of sight LENA fluxes expected at a remote orbiting spacecraft for various magnetospheric plasma regimes. This model uses measured charge exchange cross sections, either of two neutral hydrogen geocorona models, and various empirical models of the ring current and plasma sheet to calculate the contribution to the integrated directional flux from each point along the line of sight of the instrument. We discuss implications for LENA imaging of the magnetosphere based on these simulations.

1. INTRODUCTION

Magnetospheric plasma observations to date have primarily been limited to in situ single point or multipoint measurements. The wide variety of time and length scales in the magnetosphere make it highly desirable to obtain global measurements of magnetospheric plasma. As magnetospheric plasma interacts with neutral populations such as the Earth's neutral geocorona, energetic neutral atoms (ENAs) and low energy neutral atoms (LENAs) are produced by charge exchange. Global imaging of the Earth's ring current via ENAs with energies greater than approximately 30 keV has been extensively discussed[2-6]. Although this energy range is indeed important in the ring current, on many occasions there are even higher fluxes of ring current particles with energies less than a few tens of keV. Furthermore, much of the magnetosphere (e.g., the outer ring current, plasma sheet, and magnetosheath) is predominantly populated by plasmas at these lower energies. Lastly, the charge exchange cross sections for producing LENAs are larger than at higher energies.

Instrumentation advances reported recently[1] and in these proceedings (McComas et al., Funsten et al.) offer techniques for LENA detection in the energy range of <1 keV to ~50 keV. In order to help determine optimal instrument and orbital parameters, we have constructed a numerical model which calculates line of sight LENA fluxes expected on orbit for various plasma regimes. This work parallels the pioneering work of Roelof[3]. For each point along the line of sight of the instrument, we use measured charge exchange cross sections and empirical models of the neutral hydrogen geocorona, ring current, and plasma sheet to calculate their contributions to the integrated directional neutral flux. These contributions are then summed to give the line of sight LENA flux for the given look direction. We then combine multiple look direction fluxes for a specified spacecraft location into a 2 dimensional simulation image of the magnetosphere. Analysis of these images provides the anticipated LENA fluxes for optimization of instrument parameters and spacecraft orbit.

2. MODEL COMPONENTS

2.1 Algorithm

Above a few thousand kilometers altitude, the neutral geocorona is dominated by hydrogen. The unidirectional neutral flux (in units of $[cm^2\ s\ sr\ keV]^{-1}$) for species i, $f_i(E)$, is given[3] by the integral

$$f_i(E) = \sigma_{iH} \int_l J_i(r,E,\alpha)\, n_H(r)\, dl, \qquad (1)$$

where σ_{iH} is the charge exchange cross section for the interaction $i^+ + H \rightarrow i + H^+$ (i is either H^+ or O^+). The flux $J_i(r,E,\alpha)$ (units of $[cm^2\ s\ sr\ keV]^{-1}$) of magnetospheric ions is a function of location r in the magnetosphere, ion energy E, and pitch angle α relative to the local magnetic field. The neutral hydrogen number density $n_H(r)$, is given in cm^{-3} and depends on position. The integral is performed over the entire line of sight path l. This integral presupposes the medium is optically thin; i.e., the probability of a newly formed LENA undergoing a second charge exchange reaction before detection is negligible. Additionally, we do not consider electron-ion recombination or photoionization of neutralized magnetospheric ions due to their extremely small cross sections.

The inputs to the LENA model are spacecraft location, line of sight spacing (corresponding to instrument field of view), plasma species and plasma model, neutral model, energy, and integration accuracy. After the start and end points have been determined, a Romberg integration scheme with trapezoid rule[7] is used to perform the integration. The resulting neutral fluxes and the angular coordinates for each line of sight (in the spacecraft frame) are stored on disk. A commercial plotting package is then used to construct 2D images of the results.

The primary computational burden is the evaluation of the integrand at each point chosen by the integration routine along the line of sight path. The cross section is a function only of the energy and plasma species and is thus a constant over the entire path. The neutral density is stored in a lookup table for computational efficiency, so the bulk of the computation at each point is the calculation of the plasma flux. The total number of points evaluated along each path is dependent upon the variation of the integrand along the path and the integration tolerance (about 1% for the results presented here).

2.2 Neutral hydrogen geocorona models

The present model includes two different models of the neutral hydrogen geocorona based on measurements made by the ultraviolet imaging photometer flown on Dynamics Explorer I. The data were fit to spherically symmetric isothermal Chamberlain models[8] to derive optimum parameters. Preliminary results[9] were 1050° K temperature, a 600 km exobase, an exobase density of $4 \times 10^4\ cm^{-3}$, and a satellite critical level of 3.5 times the exobase radius. These parameters fit the data to 4.5 Earth radii (R_E). Beyond that, the neutral hydrogen density decreased exponentially according to $n_H = 3300\ \exp(-r / 1.46\ R_E)\ cm^{-3}$.

Subsequent analysis of a larger dataset spanning 1981 through 1985 gave revised parameters of 1050° K temperature, a 500 km exobase, an exobase density of $4.4 \times 10^4\ cm^{-3}$, and a satellite critical level of 3.0 times the exobase radius[10]. A comparison of the preliminary and revised model fits are shown in Fig. 1. The revised parameters fit the data to 12 R_E and give higher densities than the preliminary fits beyond 5 R_E. The results presented here use the revised values.

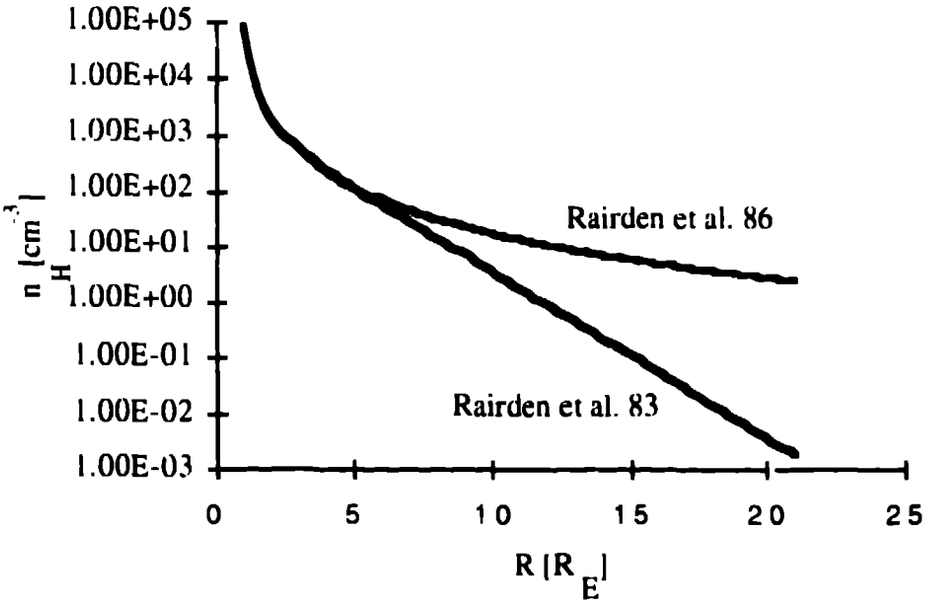

Fig. 1. Empirical neutral hydrogen geocorona densities used in the LENA model.

A fundamental question that we are attempting to answer with this model is whether the plasma sheet can be imaged using LENAs. Two important geocorona properties not presently modeled are solar cycle variability and the presence of a geotail. The neutral hydrogen density may have varied by as much as 30% [10] between 1981 and 1985. Although the exobase density rises as solar minimum is approached, the temperature falls[11]. This effect results in lower hydrogen densities at high altitudes than during solar maximum. Thus, the model results are probably more typical of solar maximum conditions and should be rescaled to predict solar minimum fluxes. A partially compensating effect that is also not modeled is the day-night asymmetry in neutral density known as the geotail. This geotail, caused by solar photon pressure, produces an observed asymmetry[10] which results in higher neutral densities in the tail than are present in our model. Thus, the model plasma sheet LENA fluxes should be slightly low for solar maximum conditions and slightly high for solar minimum conditions.

2.3 Plasma models

To compute the integral given by equation 1, it is necessary to define the plasma species and flux at every point in the magnetosphere . There are a wide variety of plasma models currently available, some of which are quite complex (as the magnetosphere undoubtedly is). We have chosen two particularly simple empirical plasma models as a starting point for this modeling - a ring current and a plasma sheet model. More complex models will be included in the future as these efforts continue.

The Earth's magnetosphere is compressed into a paraboloidal shape on the entire dayside and partially into the nightside by the solar wind. A roughly cylindrical magnetotail extends to great distances in the anti-solar direction. We use a statistically average empirical shape[12] for the magnetopause (the separatrix between magnetospheric and solar wind plasma) which is rotationally symmetric about the Sun - Earth line. The Earth's magnetic field orientation imposes deviations from rotational symmetry which are not included in this model. The model nightside ring current boundary is defined by reflecting the dayside magnetopause about the terminator. The Earth's magnetic field is approximated as a dipole within this region.

The model plasma sheet consists of a slab 2 R_E thick in the magnetic equator that extends from the nightside ring current boundary out to the tail magnetopause. The lobe regions above and below the tail plasma sheet are assumed to be empty of plasma. The model magnetosphere topology is shown in Fig. 2.

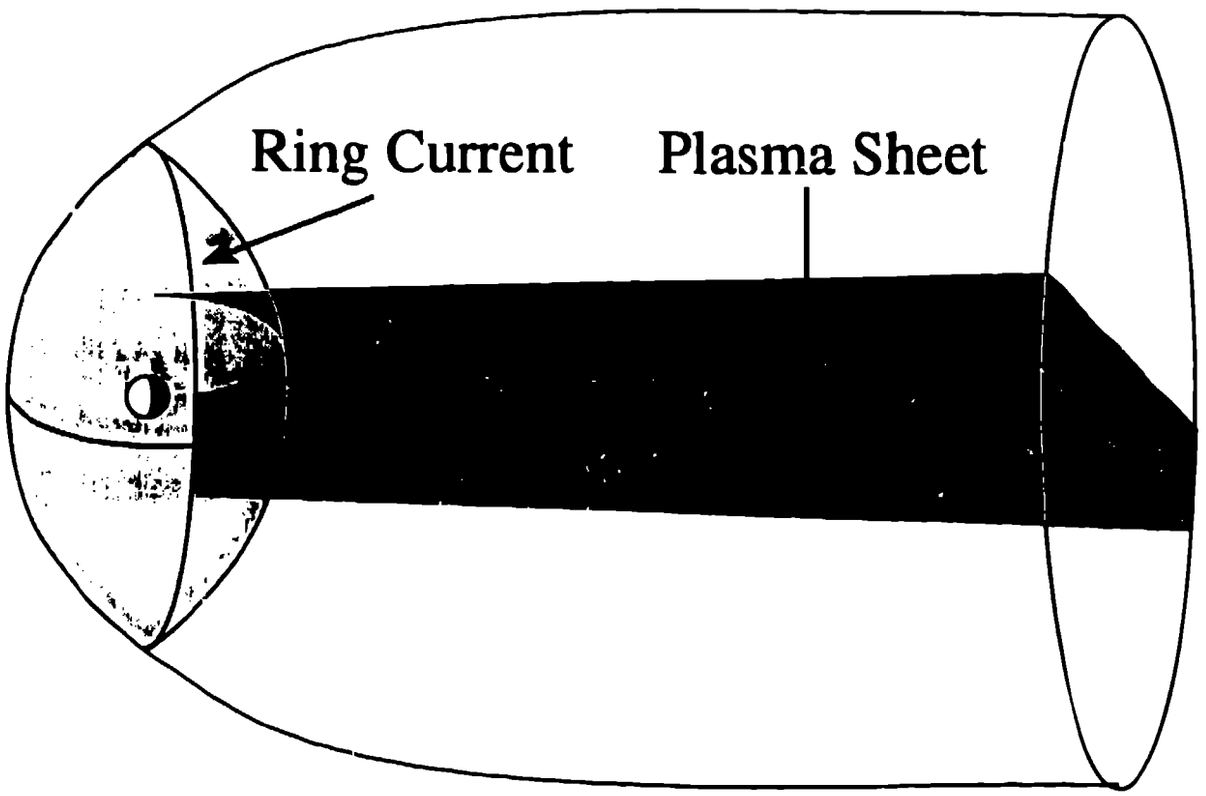

Fig. 2. Plasma regime topology used in the LENA model.

The plasma distribution within the model ring current is specified separately from the model magnetotail plasma. The two distributions are not required to match at their interface in the present model. The ring current plasma fluxes are specified along the magnetic equatorial plane and are isotropic. The ring current plasma fluxes off the magnetic equator are derived by mapping the equatorial flux along the field line using Liouville's theorem[3]. The equatorial plasma fluxes in the present model are independent of energy; energy dependence will be incorporated in the future.

Two ring current plasma species, protons and O^+, are modeled. Based on the observed radial dependence of the number density of ring current ions [13] and measured fluxes during a magnetic storm [14], we adopt empirical relations for the equatorially mirroring fluxes of ring current ions. Specifically, the proton flux during magnetically disturbed conditions (storm time) is

$$J_{\perp}^{+}(\text{storm}) \quad 1.0\times10^{6}\cdot\exp[\,0.46\cdot(R\ \ 3.5)]\ \text{for}\ R>3.5\,R_E,$$
$$1.0\times10^{6}\cdot\exp[\,3.00\cdot(3.5\ \ R)]\ \text{for}\ R\le 3.5\,R_E \qquad (2)$$

and during magnetically quiet conditions (quiet time) is

$$J_{H^+}\ (\text{quiet}) = \begin{array}{l} 1.0\text{x}10^4 \cdot \exp[-0.46 \cdot (R - 3.5)] \ \text{ for } R>3.5\ R_E\ , \\ 1.0\text{x}10^4 \cdot \exp[-3.00 \cdot (3.5 - R)] \ \text{ for } R<3.5\ R_E. \end{array} \qquad (3)$$

Similarly, the oxygen flux during magnetically disturbed conditions (storm time) is

$$J_{O^+}\ (\text{storm}) = \begin{array}{l} 1.0\text{x}10^5 \cdot \exp[-0.46 \cdot (R - 4.0)] \ \text{ for } R>4.0\ R_E\ , \\ 1.0\text{x}10^5 \cdot \exp[-3.00 \cdot (4.0 - R)] \ \text{ for } R<4.0\ R_E. \end{array} \qquad (4)$$

The quiet time O^+ ring current is probably quite small and is not modeled in the present version.

The model plasma sheet is uniformly populated with protons (mass m) having a number density n_{ps} of 0.1 cm^{-3} and a temperature Tps of 5 keV[15,16]. The flux J_{ps} is then given by

$$J_{ps} = (2E / m^2)\ f = (2E / m^2) \cdot n_{ps} \exp(-E / T_{ps}) / (T_{ps} / m)^{3/2}\ . \qquad (5)$$

where f is the plasma distribution function for a Maxwellian population.

2.4 Charge exchange cross sections

The charge exchange cross sections used in the model are derived using least squares fits to several empirical data sets which cover limited energy ranges. The cross section (σ) for the reaction $O^+ + H \rightarrow O + H^+$ has been measured for incident energies of 4 to 400 eV[17], 270 eV to 8.02 keV[18], and 11.4 to 600 keV[19]. The least squares linear fit through these data points gives

$$\sigma = (11.088 - 4.2198 \log E) \times 10^{-16}\ cm^2, \qquad 0.004\ \text{keV} < E < 600\ \text{keV}. \qquad (6)$$

The data points and Equation 6 are shown in Fig. 3.

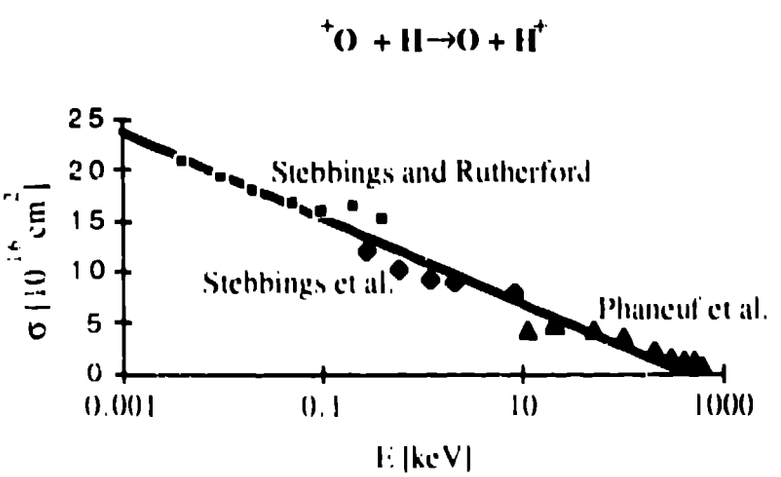

Fig. 3. Charge exchange cross section as a function of incident energy. Points are empirical data[17-19] and the line is a least squares fit to the data.

The cross section (σ) for the reaction $H^+ + H \rightarrow H + H^+$ has been measured for incident energies of 0.4 to 30 keV[20]. Theoretical considerations indicate the square root of the cross section should be a linear function of the logarithm of the velocity V. Thus, we have done the least squares linear fitting in this parameter space. The best fit through these points gives

$$\sqrt{\sigma} = (28.470 - 3.1281 \log V) \times 10^{-8} \text{ cm}, \qquad 2.8\times10^{7} \text{ cm s}^{-1} < V < 2.4\times10^{8} \text{ cm s}^{-1}. \quad (7)$$

This velocity range corresponds to the energy range 0.4 to 30 keV. The measured cross sections and best fit line as a function of energy are are shown in Fig. 4.

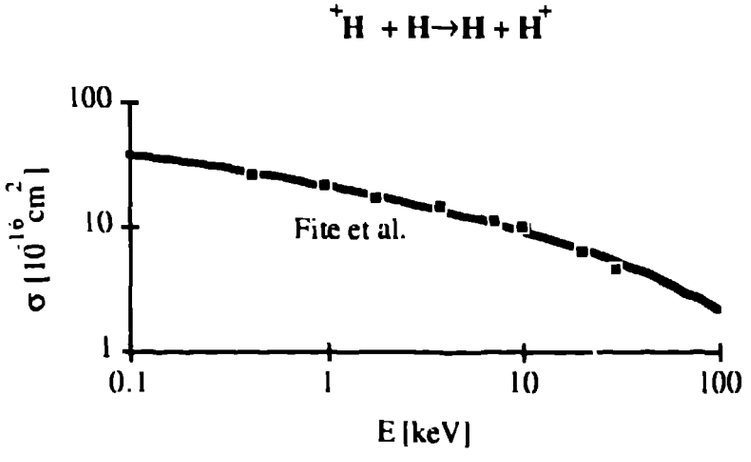

Fig. 4. Charge exchange cross section as a function of incident energy. Points are empirical data[20] and the line is a least squares fit to the data.

3. MODEL RESULTS

The output of the model is an array of neutral particle flux as a function of spacecraft polar and azimuthal angles. The polar angle is measured relative to the local (spacecraft) Z direction and the azimuthal angle is measured relative to the local X axis (positive toward the Y axis). The local X axis always points directly away from the Earth and the local Z axis is in the plane containing the spacecraft location and the magnetic dipole axis. The result is that the Earth always appears at at a polar angle of 90^0, and an azimuthal angle of 180^0.

The model outputs can be plotted as images in (polar angle, azimuthal angle) space, with a coded flux color or grayscale. Two model images with 2^0 x 2^0 resolution made at 5 keV from a spacecraft position 9 R_E to the side of the Earth and at the dipole equator are shown in Fig. 5. The top panel shows the LENA fluxes expected for a quiet time proton ring current, while the bottom panel shows the fluxes expected for a storm time ring current. The plasma sheet properties are the same in both panels. The ring current and plasma sheet are clearly visible in both panels.

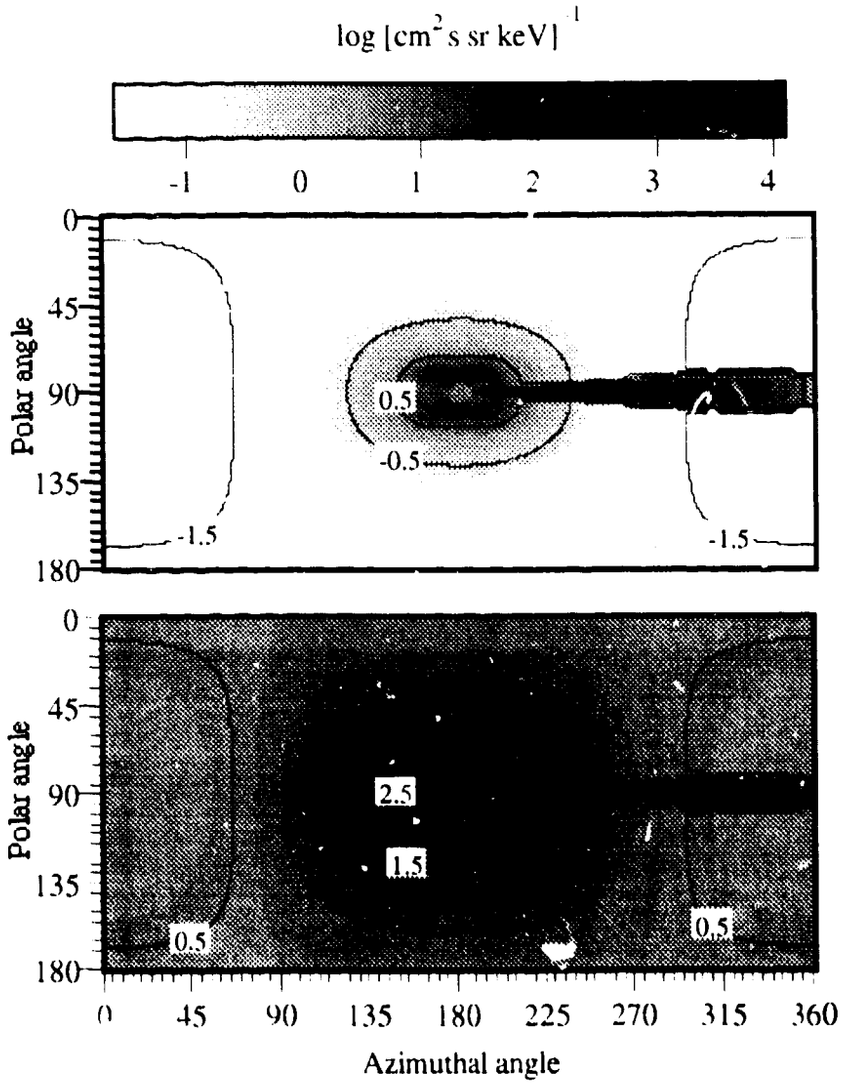

Fig. 5. Model images of the magnetosphere with quiet time (top) and storm time (bottom) ring currents. The viewpoint is from 9 R_E on thedusk side of the Earth and on the dipole magnetic equator. TheSun is at (90^o, 90^o).

The plasma sheet is believed to shrink or thin as the lobe magnetic flux builds up[22] during the growth phase[21] of a substorm, and to flap as the solar wind bulk flow direction changes and as the offset and tilted terrestrial magnetic field wobbles in space while the Earth rotates. This behavior is very difficult to detect with single point spacecraft measurements because a single spacecraft cannot usually discriminate between temporal and spatial changes. Even with a cluster of spacecraft, such effects are difficult to resolve due to a lack of synoptic information. Imaging the plasma sheet via LENAs offer the exciting possibility of separating these effects. A comparison of thin (2 R_E) and thick (6 R_E) plasma sheets from a spacecraft located at 9 R_E on the dusk side of the Earth and on the dipole magnetic equator is shown in Fig. 6. It is apparent that such plasma sheet changes are readily observable from this vantage point using LENAs.

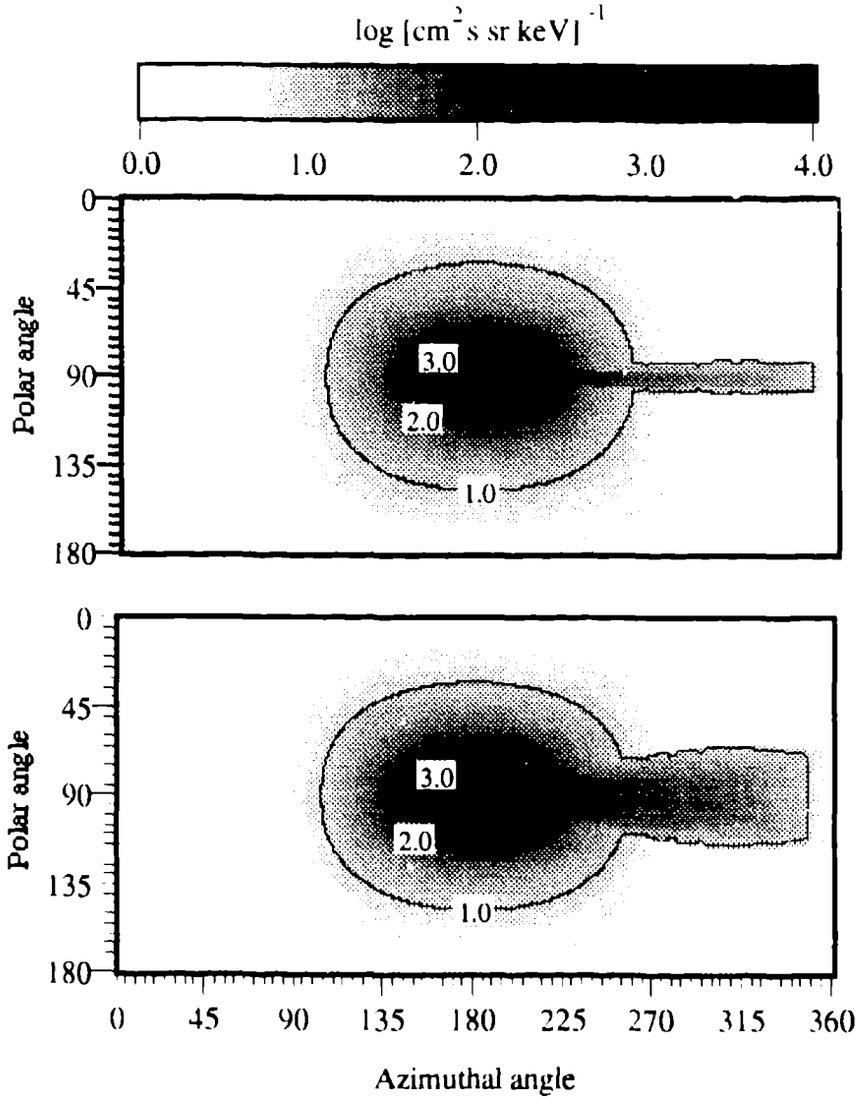

Fig. 6. Model images from a spacecraft located at 9 R_E on the dusk side of the Earth and on the dipole magnetic equator. The plasma sheet in the top panel is 2 R_E thick, while the plasma sheet is 6 R_E thick in the bottom panel.

It is also believed that the plasma sheet thins locally at some distance down the tail during the substorm growth phase, ultimately shrinking to nearly zero thickness and pinching off a plasmoid at the start of the expansion phase[22]. Two model images taken from 6.36 R_E directly down the tail and 6.36 R_E above the magnetic equatorial plane (9 R_E apogee at 45° inclination) are shown in Fig. 7. The top panel has a continuous 2 R_E thick slab plasma sheet. The bottom panel has the same plasma sheet except it has zero thickness from -15 to -20 R_E behind the Earth. The missing piece of plasma sheet is seen as the two light bands at large azimuthal and polar angles in the bottom panel.

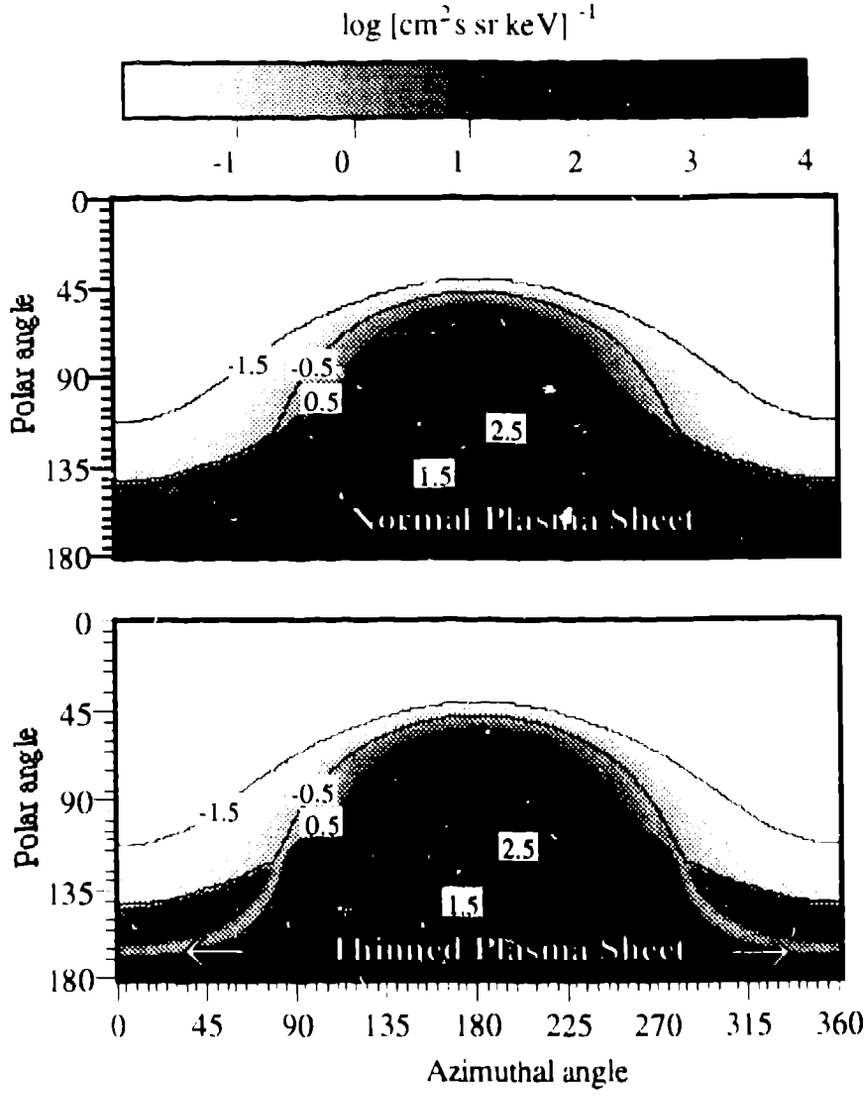

Fig. 7. Two model images made from 6.36 R_E directly down the tail and 6.36 R_E above the magnetic equatorial plane (9 R_E apogee at 45^o inclination). The bottom panel has the same plasma sheet as the top panel except the bottom panel plasma sheet has zero thickness from -15 to -20 R_E behind the Earth. This simulates the thinning of the plasma sheet near the start of the substorm expansion phase.

4. DISCUSSION

We have constructed a numerical model to calculate LENA fluxes expected at a remote orbiting spacecraft. This model uses measured charge exchange cross sections and empirical models of the geocorona, ring current, and plasma sheet. We have examined different plasma conditions from different vantage points in space to identify possible physics issues that may be addressed by a LENA imager.

We find that several important space physics issues may be addressed by a global LENA imager of sufficient resolution and sensitivity. Changes in ring current fluxes, such as enhancements during a

magnetic storm, could be observed via LENA imaging. By separately imaging hydrogen and oxygen LENAs, compositional changes in the ring current could be observable. Synoptic global information on ring current fluxes and composition would be an invaluable addition to the spacecraft measurements currently available.

The modeling results presented here indicate the exciting possibility of imaging the plasma sheet. The magnetotail is very dynamic and inextricably linked with substorm dynamics. Direct imaging of plasma sheet thinning and plasma disconnection (plasmoid formation) would constitute a tremendous step forward in our efforts to identify and quantify magnetotail morphology during substorms. The plasma sheet is, however, more difficult to image than the ring current and the lower LENA fluxes pose a considerable challenge for potential imagers. Instruments will need to be highly optimized to obtain sufficient sensitivities for this task. Further, the spacecraft orbit chosen is critical, and optimal orbital parameters are the subject of continuing work.

The results of our modeling indicate that LENA imaging of the ring current and plasma sheet are indeed feasible and that the scientific gains from such measurements would be immediate and significant. Much more simulation needs to be performed to obtain basic information on LENA imaging. We are developing advanced models based on the simulations presented here to investigate, for example, optimal orbit parameters, other regions of the magnetosphere which might be imaged, and the viability of magnetospheric tomography using multiple spacecraft.

5. ACKNOWLEDGEMENTS

We thank Galen Gisler, Rick Elphic, and Geoff Reeves of the Los Alamos Space Physics Group for invaluable discussions, support, and enthusiasm. This work was carried out under the auspices of the United States Department of Energy.

6. REFERENCES

1. D. J. McComas, B. L. Barraclough, R. C. Elphic, H. O. Funsten III, and M. F. Thomsen, "Magnetospheric Imaging With Low-energy Neutral Atoms", *Proc. Natl. Acad. Sci. USA*, **88**, 9598-9602, 1991

2. E. C. Roelof, D. G. Mitchell, and D. J. Williams, "Energetic Neutral Atoms (E ~ 50 keV) From the Ring Current: IMP 7/8 and ISEE 1", *J. Geophys. Res.*, **90**, 10991-11008, 1985

3. E. C. Roelof, "Energetic Neutral Atom Image From a Storm-Time Ring Current", *Geophys. Res. Lett.*, **14**, 652-655, 1987

4. R. W. McEntire and D. G. Mitchell, "Instrumentation for Global Magnetospheric Imaging via Energetic Neutral Atoms", *Geophys.. Monogr. Ser.*, **54**, 69-80, 1989

5. E. P. Keath, G.B. Andrews, A. F. Cheng, S. M. Krimigis, B. H. Mauk, D. G. Mitchell, and D. J. Williams, "Instrumentation for Energetic Neutral Atom Imaging of Magnetospheres", *Geophys. Monogr. Ser.*, **54**, 165-170, 1989

6. C. C. Curtis and K. C. Hseih, "Remote Sensing o. Planetary Magnetospheres: Imaging via Energetic Neutral Atoms", *Geophys. Monogr. Ser.*, **54**, 247-251, 1989

7. W. H. Press, B. P. Flannery, S. A. Teukolsky, and W. T. Vetterling, Numerical Recipes in C, Cambridge University Press, Cambridge, 119-125, 1988

8. J. W. Chamberlain, "Planetary Coronae and Atmospheric Evolution", *Planet. Space Sci.*, **11**, 901-960, 1963

9. R. L. Rairden, L. A. Frank, and J. D. Craven, "Geocoronal Imaging With Dynamics Explorer: A First Look", *Geophys. Res. Lett.*, **7**, 533-536, 1983

10. R. L. Rairden, L. A. Frank, and J. D. Craven, "Geocoronal Imaging With Dynamics Explorer", *J. Geophys. Res.*, **91**, 13,613-13,630, 1986

11. A. E. Hedin, "A Revised Thermospheric Model Based on Mass Spectrometer and Incoherent Scatter Data: MSIS-83", *J. Geophys. Res.*, **88**, 10,170-10,188, 1983

12. D. H. Fairfield, "Average and Usual Locations of the Earth's Magnetopause and Bow Shock", *J. Geophys. Res.*, **76**, 6700-6716, 1971

13. G. Gloeckler, B. Wilken, W. Stüdemann, F. M. Ipavich, D. Hovestadt, D. C. Hamilton, and G. Kremser, "First Composition Measurement of the Bulk of the Storm-Time Ring Current (1 to 300 keV/e) With AMPTE/CCE", *Geophys. Res. Lett.*, **12**, 325-328, 1971

14. S. M. Krimigis, G. Gloeckler, R. W. McEntire, T. A. Potemra, F. L. Scarf, and E. G. Shelley, "Magnetic Storm of September 4, 1984: A Synthesis of Ring Current Spectra and Energy Densities Measured With AMPTE/CCE", *Geophys. Res. Lett.*, **12**, 329-332, 1985

15. A. T. Y. Lui, "Road Map to Magnetotail Domains", Magnetotail Physics, Johns Hopkins University Press, Baltimore and London, 3-9, 1987

16. W. Lennartsson, "Dynamical Features of the Plasma-Sheet Ion Composition, Density, and Energy", Magnetotail Physics, Johns Hopkins University Press, Baltimore, 35-40, 1987

17. R. F. Stebbings and J. A. Rutherford, "Low-Energy Collisions Between $O^+(^4S)$ and H(1s)", *J. Geophys. Res.*, **73**, 1035-1038, 1968

18. R. F. Stebbings, W. L. Fite, and D. G. Hummer, "Charge Transfer Between Atomic Hydrogen and N^+ and O^+", *J. Chem. Phys.*, **33**, 1226-1233, 1960

19. R. A. Phaneuf, F. W. Meyer, and R. H. McKnight, "Single-Electron Capture by Multiply Charged Ions of Carbon, Nitrogen, and Oxygen in Atomic and Molecular Hydrogen", *Phys. Rev. A*, **17**, 534-545, 1978

20. W. L. Fite, R. F. Stebbings, D. G. Hummer, and R. T. Brackman, "Ionization and Charge Transfer in Proton-Hydrogen Atom Collisions", *Phys. Rev.*, **119**, 663-668, 1960

21. R. L. McPherron, "Growth Phase of Magnetospheric Substorms", *J. Geophys. Res.*, **75**, 5592-5599, 1970

22. e.g., D. N. Baker, S.-I. Akasofu, W. Baumjohann, J. W. Bieber, D. H. Fairfield, E. W. Hones, Jr., B. Mauk, R. L. McPherron, and T. E. Moore, Substorms in the magnetosphere, Solar Terrestrial Physics: Present and Future, NASA Reference Pub. 1120, 1984